

Evaluating Text-to-Image Synthesis with a Conditional Fréchet Distance

Jaywon Koo*, Jefferson Hernandez*, Moayed Haji-Ali, Ziyan Yang, and Vicente Ordonez
Rice University

{jk125, jefehern, mh155, zy47, vicenteor}@rice.edu

<https://github.com/JaywonKoo17/cFreD>

Abstract

Evaluating text-to-image synthesis is challenging due to misalignment between established metrics and human preferences. We propose cFreD, a metric based on the notion of Conditional Fréchet Distance that explicitly accounts for both visual fidelity and text-prompt alignment. Existing metrics such as Inception Score (IS), Fréchet Inception Distance (FID) and CLIPScore assess either image quality or image-text alignment but not both which limits their correlation with human preferences. Scoring models explicitly trained to replicate human preferences require constant updates and may not generalize to novel generation techniques or out-of-domain inputs. Through extensive experiments across multiple recently proposed text-to-image models and diverse prompt datasets, we demonstrate that cFreD exhibits a higher correlation with human judgments compared to statistical metrics, including metrics trained with human preferences. Our findings validate cFreD as a robust, future-proof metric for the systematic evaluation of text-to-image models, standardizing benchmarking in this rapidly evolving field. We release our evaluation toolkit and benchmark in the appendix.

1. Introduction

Generative models have demonstrated remarkable capabilities in text-to-image generation [17, 24, 53, 59], text-to-video generation [5, 35, 37, 60, 78], and other modalities [4, 25, 26, 28, 47, 82]. This progress has been driven by technical breakthroughs such as the development and improved understanding of Generative Adversarial Networks (GANs) [22], Variational AutoEncoders (VAEs) [32], and more recently models based on Denoising Diffusion [65] and Flow Matching [43]. Automatic evaluation metrics have played a crucial role in guiding the development and refinement of these models by offering quantitative benchmarks that compare the quality, diversity, and fidelity of various

*Equal contribution.

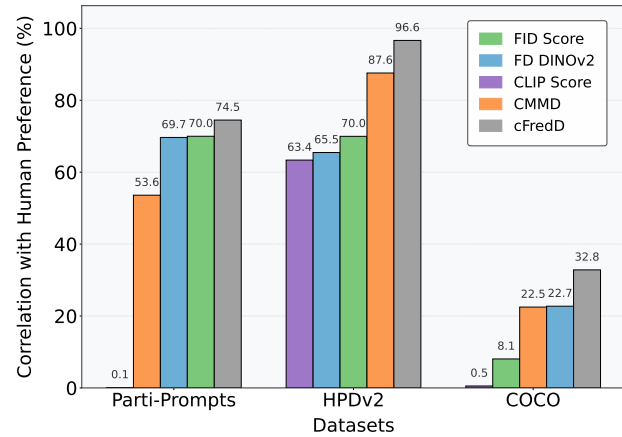


Figure 1. Correlation of five evaluation metrics with human preferences on three benchmark datasets (Parti-Prompts, HPDv2, and COCO). Compared to FID, FD_{DINOv2}, CLIPScore, and CMMD, our proposed method (cFreD) achieves consistently higher correlation with human judgments across all datasets.

generative approaches. The most commonly used metrics include Inception Score (IS) [62], Fréchet Inception Distance (FID) [30], and CLIPScore [29].

We consider that it is time to reassess evaluation metrics for text-to-image synthesis and propose cFreD, based on a conditional formulation of Fréchet Distance. Prior work has reported that existing metrics exhibit weak correlation with human preferences [34, 46, 74, 76]. Additionally, metrics such as IS or FID, although indicative of image quality to some extent, do not measure the alignment of generated images with input text prompts, focusing solely on comparing the generated image distributions with respect to a reference set [3]. For instance, consider a dataset with two images: one of a *dog* and one of a *cat*, each paired with their corresponding prompt. A perfect text-to-image model that mistakenly swaps these mappings (*i.e.* generating a *cat* for *dog* prompt and vice versa) would achieve near zero FID since the overall distribution of cats and dogs is maintained, despite the misalignment with the intended prompts. We show that cFreD captures better image quality assessment and conditioning

on input text and results in improved correlation with human preferences (see Fig. 2).

Currently, the most reliable form of evaluation for text-to-image models relies on collecting human preference data through crowd-sourcing, similar to the way Large Language Models (LLMs) are evaluated (i.e. the LMSys Arena [10]). For instance, the Parti Prompts Arena [49] employs 1,600 English prompts originally designed for assessing Parti models [79], presenting users with a gamified task of selecting their preferred image from two random outputs generated by four different models played over 10 rounds. Similarly, the Text-to-Image Arena Leaderboard [1] asks users to compare the outputs from two randomly selected models given a prompt, and their preferences are used to calculate *ELO* scores. However, collecting enough human preference data to statistically establish model superiority is time-intensive, and these arenas risk becoming unmaintained over time, as evidenced by the Parti Prompts Arena, which no longer collects votes. Recent work has also proposed learning metrics directly from human preferences [34, 73, 74, 76, 85]. However, it remains unclear whether such metrics trained on data from previous generative models can effectively assess the next generation of models. Moreover, since human preferences are inherently dynamic and evolve over time, these models risk becoming outdated unless they are regularly updated with fresh preference data. As a result, metrics such as FID, CLIPScore and our proposed cFreD will continue to play an important role in model evaluation.

Most related to our work is the previously proposed conditional Fréchet Inception Distance (cFID) by Soloveitchik et al. [66]. Unlike traditional statistical metrics, cFID incorporates a conditioning modality to evaluate not only visual quality but also alignment with respect to an input condition. We revisit and apply this formulation, originally proposed to evaluate image-to-image generation, to text-to-image generation. Furthermore, we systematically analyze how the choice of vision and text backbone models affect metric performance and demonstrate that the previously used Inception V3 [69] model is an outdated choice. By replacing it with a superior backbone model, we propose cFreD as a superior alternative to other statistical metrics (see Fig. 1).

Our contributions can be summarized as follows:

- We demonstrate that a metric based on Conditional Fréchet Distance (cFreD) is a powerful alternative to the more common practice of evaluating text-to-image models with a combination of FID and CLIPScore.
- We show that cFreD correlates strongly with human evaluations, outperforming previous statistical metrics on three major human preference datasets.
- We open-source our evaluation toolkit and offer the community a unified version of the Partiprompts Arena.

2. Related Work

Text-to-Image Generation Metrics. Text-to-image generation aims to synthesize images conditioned on natural language descriptions. This field has evolved significantly since the early work on GAN-based models [77, 81]. More recently, diffusion models (e.g., GLIDE [48], Imagen [61]) and autoregressive architectures (e.g., DALL-E [57]) have achieved the state-of-the-art in generating high-quality, semantically consistent images.

Evaluating the quality of generated images typically relies on metrics like the Fréchet Inception Distance (FID [30]) and Inception Score (IS) [62], which primarily assess image realism and diversity. However, these metrics often correlate poorly with human perception and do not capture alignment between generated images and their corresponding text prompt [31]. In response, several alternative metrics have been introduced. For instance, CLIPScore [29]—which leverages the joint vision-language embeddings of the CLIP model has gained popularity as a measure of semantic consistency between images and text. Other recent proposals include CMMD [31], a metric that uses CLIP embeddings combined with Maximum Mean Discrepancy (MMD) computed with a Gaussian RBF kernel, and FD_{DINOv2} [67], which is based on the finding that the DINOv2-ViT-L/14 model yields more expressive feature representations for evaluation. FWD [70] is another approach that measures the similarity between generated and real images by computing the Fréchet Distance over their wavelet coefficients. Moreover, perceptual metrics such as LPIPS [83] have been used to assess image similarity, although they do not consider the semantic alignment provided by the input text.

While these methods have advanced the evaluation of text-to-image generation, they still fall short in fully capturing human preferences—particularly regarding the interplay between image quality and text-image alignment. In contrast, our proposed metric (cFreD) integrates the text input directly into the evaluation process, thus offering a better human-aligned metric for assessing text-to-image synthesis.

Evaluating with Human Preferences. Recent research in text-to-image evaluation has focused on incorporating human preferences to assess the quality of generated images with their corresponding textual prompts [20, 34, 36, 51, 73, 74, 76, 84, 85]. In this line of work, human preference datasets are constructed where generated images are annotated with scores or rankings based on human judgments. These annotations allow the fine-tuning of vision-language models (VLMs) to predict human preferences by analyzing both the image and its accompanying text. HPS [74] directly collects data from discord servers of generated images, creating a dataset of 98k images labeled as *preferred* and *dispreferred* and uses this data to fintune a CLIP-L/14 model to maximize the similarity of *preferred* images with

Prompt: "A living room with a couch and a laptop computer resting on the couch."



Figure 2. Comparison of image rankings across different evaluation metrics for the prompt 'A living room with a couch and a laptop computer resting on the couch.' Each row displays how images are ranked from 1 to 9 according to a specific metric (Human preference, FID, CLIP, CMMD, ImageReward, and cFreD), illustrating how different metrics prioritize distinct visual qualities. Inside a **green** box is the highest rated model as judged by human preferences (FLUX.1-dev) and inside a **purple** box is the lowest rated model as judged by human preferences (SDv1.5). cFreD is the only statistical metric that preserves their relative ordering.

the prompt while minimizing the similarity for the *dispreferred* images. PickScore [34] creates a web-app and collects a dataset of $\sim 500k$ images generated from various diffusion models and is used in a similar manner to train a CLIP-H/14 model to maximize the similarity of the preferred images with their prompt. ImageReward [76] collects $\sim 137k$ data points from DiffusionDB [71] for annotators to create *preferred* and *dispreferred* pairs. A reward model is then trained for text-to-image synthesis evaluation. HPSv2 [73] collects 108k data points from DiffusionDB [71] and COCO captions. Then, the prompts are cleaned using GPT-4 and

annotators are asked to rank between images from four diffusion models. OpenCLIP-H/14 is fine-tuned to maximize the similarity of the preferred image with the prompt. Moreover, MPS [84] collects 66k preference data points from various sources [54, 71]. Prompts are refined and augmented using GPT-4. Annotators are asked to rank images across four dimensions. Finally, a multi-aspect scoring model is trained to evaluate generated images across aesthetics, alignment, and detail.

Despite the promise of these human preference-based approaches, they require extensive human-annotated datasets

Models	Statistical Metric												Human Preference Trained Metric							
	Human↑		FID↓		FD _{DINOv2} ↓		CLIP↑		CMMD↓		cFreD↓		Aesthetic↑		ImReward↑		HPS v2↑		MPS↑	
	R#	Rate	R#	Score	R#	Score	R#	Score	R#	Score	R#	Score	R#	Score	R#	Score	R#	Score	R#	Score
<i>GLIDE</i> [48]	1	80.87%	1	7.90	1	6.88	9	14.34	1	2.42	1	3.79	1	5.55	3	0.37	2	25.52	1	12.72
<i>COCO</i> [42]	2	80.66%	7	13.11	7	13.05	10	13.11	5	15.07	4	4.55	5	5.03	1	0.55	1	25.64	5	10.92
<i>FuseDream</i> [44]	3	76.29%	2	8.39	2	7.59	5	15.07	4	5.41	2	4.16	4	5.34	2	0.47	3	24.40	2	12.44
<i>DALLE 2</i> [58]	4	75.87%	3	9.16	3	7.95	8	14.39	3	4.06	3	4.42	3	5.40	6	0.07	5	23.81	4	11.75
<i>VQGAN+CLIP</i> [16]	5	68.78%	4	10.11	4	8.70	7	14.41	2	3.70	5	4.90	2	5.40	5	0.08	4	23.93	3	11.82
<i>CogView2</i> [14]	6	39.00%	6	12.65	6	12.87	3	15.45	8	45.64	7	6.93	7	4.82	7	0.02	7	19.45	7	8.85
<i>SDv1.4</i> [59]	7	38.36%	5	12.51	5	11.93	4	15.42	6	28.52	8	7.18	8	4.56	8	-0.67	8	19.44	8	8.00
<i>VQ-Diffusion</i> [23]	8	32.04%	8	13.85	8	13.12	6	14.71	7	33.40	6	6.59	6	4.88	4	0.17	6	21.91	6	10.15
<i>SDv2.0</i> [59]	9	22.00%	9	14.74	9	14.23	2	15.62	10	55.88	9	8.16	9	4.54	9	-0.72	9	18.45	9	7.24
<i>LAFITE</i> [86]	10	9.07%	10	15.12	10	14.63	1	16.01	9	53.22	10	9.06	10	4.23	10	-1.45	10	15.03	10	5.08
ρ^2	-	0.70	0.65	0.63	0.88	0.97	0.83	0.71	<u>0.90</u>	0.86										
Rank Acc.	-	86.7	86.7	15.6	80.0	91.1	82.2	84.4	<u>88.9</u>	86.7										

Table 1. Text-to-image model ranking and scores by statistical models (FID, FD_{DINOv2}, CLIP score, CMMD, and cFreD) and models that were trained with human preference (Aesthetic Score, ImageReward, HPSv2, and MPS) on HPDv2 test set. Best results in **bold**, second best underlined

that are time-consuming and labor-intensive to construct. Since these methods often train on images from specific text-to-image synthesis models, they may not work well for newer models as the metric might prefer outputs for existing models. Furthermore, because these preference-trained models typically rely on real-world data, they do not effectively adapt to the model development process when researchers train on smaller datasets such as CIFAR-100 or synthetic data, nor do they easily transfer to specialized domains such as aerial or medical imaging. In contrast, cFreD does not require additional training or human preference data, yet it effectively incorporates textual context during evaluation and can be readily applied to new data.

3. Methodology

In this work, we evaluate text-to-image synthesis using a conditional variant of the Fréchet Distance (FD). This formulation was also proposed in the work of Soloveitchik et al. [66] as a conditional version of the FID metric. For succinctness, we offer here a review of this formulation. Unlike the standard Fréchet Distance (FD) which only compares the marginal distributions of real and generated images, *conditional FD* accounts for the conditioning provided by a text prompt x .

3.1. Conditional Fréchet Distance

For a given prompt x , we assume that the real image y and the generated image \hat{y} are drawn from the conditional distributions

$$\begin{aligned} Q_{y|x} &= \mathcal{N}(\mu_{y|x}, \Sigma_{yy|x}), \\ Q_{\hat{y}|x} &= \mathcal{N}(\mu_{\hat{y}|x}, \Sigma_{\hat{y}\hat{y}|x}), \end{aligned} \quad (1)$$

where $\mu_{y|x}$ and $\mu_{\hat{y}|x}$ are the conditional means, and $\Sigma_{yy|x}$ and $\Sigma_{\hat{y}\hat{y}|x}$ are the conditional covariance matrices. These statistics capture the distribution of images corresponding to the text prompt.

Following the derivation in [66], the conditional Fréchet Distance is defined as the expectation over the prompts of the distance between the two conditional Gaussian distributions:

$$\begin{aligned} \text{cFreD} = & \mathbb{E}_x \left[\|\mu_{y|x} - \mu_{\hat{y}|x}\|^2 \right. \\ & \left. + \text{Tr} \left(\Sigma_{yy|x} + \Sigma_{\hat{y}\hat{y}|x} - 2 \left(\Sigma_{yy|x}^{1/2} \Sigma_{\hat{y}\hat{y}|x} \Sigma_{yy|x}^{1/2} \right)^{1/2} \right) \right]. \end{aligned}$$

An equivalent formulation can be derived that expresses cFreD in terms of the unconditional moments and the cross-covariances:

$$\begin{aligned} \text{cFreD} = & \|\mu_y - \mu_{\hat{y}}\|^2 + \text{Tr} \left[(\Sigma_{yx} - \Sigma_{\hat{y}x}) \Sigma_{xx}^{-1} (\Sigma_{xy} - \Sigma_{x\hat{y}}) \right] \\ & + \text{Tr} \left[\Sigma_{yy|x} + \Sigma_{y\hat{y}|x} - 2 \left(\Sigma_{yy|x}^{1/2} \Sigma_{y\hat{y}|x} \Sigma_{yy|x}^{1/2} \right)^{1/2} \right]. \end{aligned}$$

In these expressions, μ_y and $\mu_{\hat{y}}$ are the unconditional means of the real and generated images, respectively. In contrast, Σ_{yx} and $\Sigma_{x\hat{y}}$ denote the cross-covariances with the input prompt x .

By incorporating the prompt x , cFreD simultaneously measures (1) the realism of the generated images (via the comparison of unconditional statistics) and (2) the fidelity of the generated images with respect to the text prompt (via the conditional moments and cross-covariances). Thus, cFreD

Models	Statistical Metric												Human Preference Trained Metric							
	Human↑		FID↓		FD _{DINOv2} ↓		CLIP↑		CMMD↓		cFreD↓		Aesthetic↑		ImReward↑		HPS v2↑		MPS↑	
	R#	Rate	R#	Score	R#	Score	R#	Score	R#	Score	R#	Score	R#	Score	R#	Score	R#	Score	R#	Score
<i>SDXL</i> [53]	1	69.84%	1	31.24	1	23.50	2	32.79	1	2.55	1	2.98	3	5.64	1	0.95	1	28.63	4	10.33
<i>Kand2</i> [64]	2	46.10%	2	32.08	2	24.35	3	32.62	2	2.77	2	3.21	2	5.65	2	0.90	2	28.13	2	11.29
<i>Wuerst</i> [52]	3	42.68%	3	38.43	3	30.93	4	31.72	3	3.83	3	4.18	1	5.71	3	0.79	3	27.79	1	11.30
<i>Karlo</i> [40]	4	29.21%	4	48.40	4	41.57	1	33.01	4	19.95	4	5.45	4	4.93	4	0.70	4	26.56	3	11.11
ρ^2	-			0.70		0.70		0.12		0.54		0.73		0.43		<u>0.81</u>		0.83		0.65

Table 2. Text-to-image model ranking and scores by statistical metrics (FID, FD_{DINOv2}, CLIP score, CMMD, and cFreD) and models that were trained with human preference (Aesthetic Score, ImageReward, and MPS) on Parti-Prompt. Best results in **bold**, second best underlined

provides a more comprehensive evaluation metric for text-to-image models compared to traditional FID, which may fail to penalize cases where a model produces realistic images that are uncorrelated with the input prompt.

4. Experiment Settings

We evaluate the alignment of our proposed metric cFreD with human preferences and compare it against standard evaluation metrics. In this section we introduce the experimental setup (Sec. 4.1), and report the results (Sec. 4.2).

4.1. Experimental Setup

Dataset. To evaluate how correlated our metric is with human preferences, we need rankings of generated images from different models using the same prompt. We use HPDv2 test set [73] and Parti Prompts Arena. HPDv2 [73] test set contains nine different generated images (each from a different model) and one real image from COCO [6] for each prompt. Parti Prompts Arena [49] has 1,600 generated images, each from four different models. We gather the scattered Parti Prompts data on the web and consolidate it into a unified version. However, since the real image does not consistently receive the highest human preference, we took the most preferred image for each prompt and designated it as the reference image. To evaluate recent models, we randomly selected 1,000 prompts from the COCO train and validation sets, ensuring these prompts were not part of the HPDv2 training and testing sets. For each prompt, we generated images using nine models listed on the Arena Leaderboard [1]. The original COCO images serve as reference images in this evaluation.

Metric Comparison & Evaluation Setting. We compare cFreD against four standard statistical metrics (FID [30], FD_{DINOv2} [67], CLIPScore [29], and CMMD [31]). We also compare with four models that were trained with human preference data (Aesthetic Score [63], ImageReward [76], HPSv2 [73], and MPS [84]). We evaluate human correlation from both ranking and scoring perspectives. For each metric,

we report the scores and rankings of the models and calculate the correlation with human evaluation results. cFreD uses DINOv2-G/14¹ for image embedding and the OpenCLIP ConvNext-B Text Encoder² for text embeddings.

Rank Accuracy. This metric quantifies the proportion of correctly ordered pairs—that is, it represents the probability that a randomly selected pair is concordant with the true rank. Previous works on learning human preferences [63, 73, 76, 84] measure performance using per item rank accuracy, which computes the ranking accuracy for each image-text pair and then averages the results. In contrast, cFreD evaluates the overall ranking performance across the entire dataset by computing a global rank accuracy. For statistical metrics [29–31, 67], we follow this convention and derive rankings directly from their raw scores. For human preference-trained metrics, we first average the ranking each model receives over all samples and then determine the final ranking based on these averages.

4.2. Results

Results on HPDv2. Table 1 summarizes the rankings and scores for images generated by various models—including one real image—across multiple evaluation metrics. Notably, cFreD achieves the highest alignment with human preferences, reaching a correlation of 0.97. Among statistical metrics, cFreD attains the highest correlation and is comparable to HPSv2 (0.94), a model explicitly trained on human preferences. Given that HPSv2 was trained on the HPSv2 training set, which includes four models from the test set, and employed the same annotators, it inherently encodes specific human preference biases of the same setting. In contrast, cFreD achieves comparable or superior correlation with human evaluation without any human preference training. These results demonstrate that cFreD provides more reliable rankings across diverse models compared to standard automatic metrics and metrics trained explicitly on human preference data.

¹timm.vit.giant_patch14_dinov2.lvd142m

²convnext_base_w_laion2b_s13b_b82k_augreg

Models	Statistical Metric										Human Preference Trained Metric									
	Humans↑		FID↓		FD _{DINOv2} ↓		CLIP↑		CMMMD↓		cFreD↓		Aesthetic↑		ImReward↑		HPS v2↑		MPS↑	
	R#	ELO	R#	Score	R#	Score	R#	Score	R#	Score	R#	Score	R#	Score	R#	Score	R#	Score		
<i>FLUX.I/dev</i> [38]	1	1083	5	10.45	7	7.21	9	30.72	8	6.08	4	9.93	2	5.75	3	1.10	2	30.74	2	12.90
<i>SDv3.5-L Turbo</i> [17]	2	1073	9	11.68	9	8.12	6	31.11	7	48.52	7	10.44	6	5.50	6	0.64	7	26.52	6	10.88
<i>SDv3.5-L</i> [17]	3	1069	2	10.27	4	6.77	1	31.74	4	40.27	2	9.49	4	5.55	2	1.10	3	30.07	3	12.30
<i>Playgroundv2.5</i> [41]	4	997	7	10.90	8	7.50	7	31.03	9	66.10	5	10.08	1	6.16	1	1.15	1	31.56	1	13.15
<i>SDv3-M</i> [17]	5	944	6	10.46	5	7.09	3	31.68	2	34.34	1	9.49	7	5.45	4	1.08	4	29.80	9	2.35
<i>SDXL</i> [53]	6	890	3	10.31	2	6.66	2	31.70	6	45.07	3	9.73	3	5.61	5	0.76	5	28.34	4	12.08
<i>SDv2.1</i> [59]	7	752	1	10.14	1	6.55	4	31.42	3	35.17	6	10.24	5	5.52	8	0.41	6	26.58	5	10.90
<i>Janus Pro</i> [8]	8	740	8	10.97	6	7.17	8	30.99	5	43.51	9	10.76	9	5.33	7	0.57	8	26.22	7	10.70
<i>SDv1.5</i> [59]	9	664	4	10.41	3	6.73	5	31.21	1	29.89	8	10.58	8	5.34	9	0.19	9	26.15	8	10.50
ρ^2	-		0.08	0.29	0.00		0.22	0.33		0.27		0.69		<u>0.48</u>		<u>0.48</u>				
Rank Acc.	-		41.67	36.11	47.22		30.56	66.67		<u>72.22</u>		80.56		80.56		80.56				

Table 3. Text-to-image model ranking by automatic models(FID, FD_{DINOv2}, CLIP score, CMMMD, and cFreD) and models that were trained with human preference (Aesthetic Score, ImageReward, HPSv2, and MPS) on randomly sampled COCO prompts. Rank Acc. below 0.5 indicates there are more discordant pairs than concordant ones. Best results in **bold**, second best underlined

Table 1 also reports the rank accuracy scores on the HPDv2 test set. Among all evaluated metrics, cFreD achieves the highest rank accuracy (91.1%), highlighting its strong correspondence with human judgments. HPSv2 follows as the second-best metric with an accuracy of 88.9%, while both FID and FD_{DINOv2} obtain competitive scores of 86.7%. Overall, although models trained with human preference data tend to align well with human judgments, cFreD emerges as the most robust and reliable metric.

Result on PartiPrompts Arena. Table 2 presents the rankings and scores of text-to-image models evaluated on the Parti-Prompt Arena using both statistical metrics and human preference-trained models. Among the statistical metrics, cFreD achieves the highest correlation with human evaluations (0.73), with FID and FD_{DINOv2} both reaching a correlation of 0.70. In contrast, the CLIP score shows a very low correlation (0.12) with human judgments. In the human preference trained category, HPSv2 has the strongest alignment, achieving the highest correlation (0.83), followed by ImageReward (0.81) and MPS (0.65). These results highlight that while cFreD is a robust automatic metric, HPSv2 stands out as the most effective in capturing human evaluation trends in the PartiPrompts Arena.

Results on COCO. Table 3 presents an evaluation on the COCO dataset using nine modern text-to-image models, with human preference rankings sourced from the Text-to-Image Leaderboard and expressed as ELO scores. Among statistical metrics (FID, FD_{DINOv2}, CLIP, CMMMD, and our proposed cFreD), only cFreD exhibits a strong correlation with human preferences, achieving a correlation of 0.33 and a non-trivial rank accuracy of 66.67%. This result places cFreD as the third most aligned metric overall, surpassed

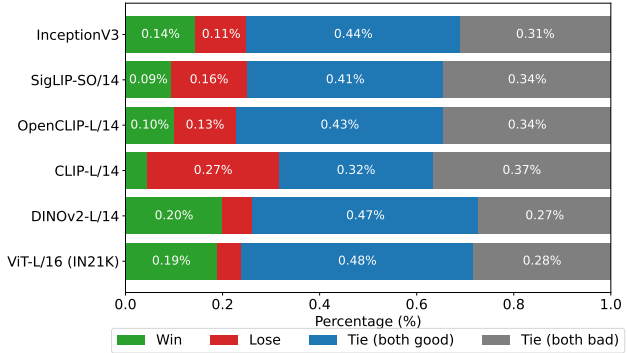


Figure 3. **Win rates** between the concordance of the true rank against the ranking created by each image backbone when evaluated on the COCO dataset.

only by the human preference-trained metrics ImageReward, HPSv2, and MPS. Notably, all other statistical metrics show considerably weaker alignment with ELO rankings and, as a result, inverted the rankings, resulting in a Rank Acc. below 0.5. These findings highlight that cFreD is sensitive to both visual fidelity and prompt consistency, reinforcing its value as a practical, training-free alternative for benchmarking text-to-image generation.

Fig. 2 shows how different evaluation metrics (FID, CLIP, CMMMD, ImageReward, and cFreD) rank the same set of images from best to worst for the prompt, with human preferences highlighting the best (green box) and worst (purple box) outputs. Notably, cFreD is the only statistical metric that preserves the human-chosen ordering.

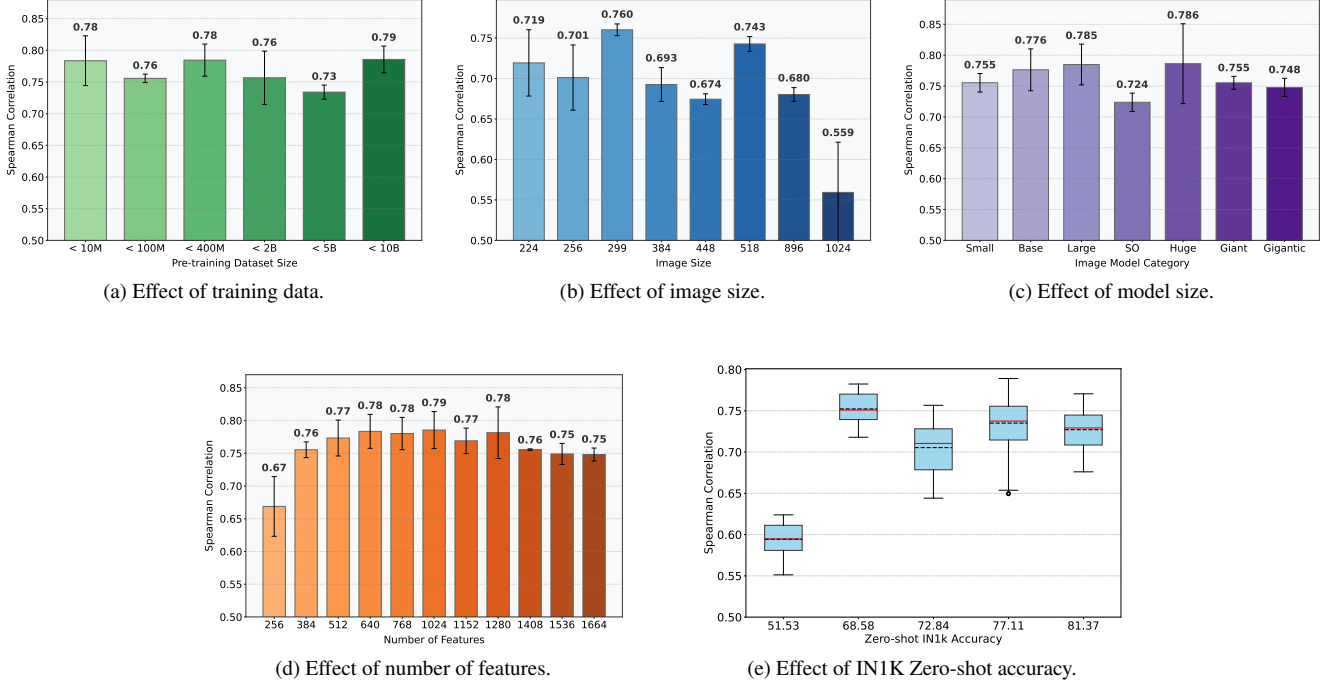


Figure 4. **Ablation study on the Parti-Prompts** dataset comparing the correlation to human preferences under varying factors: (a) the ViT training dataset, (b) input image size, (c) model capacity, (d) the number of features in the last ViT layer, and (e) zero-shot accuracy on ImageNet-1K.

4.3. Are we done with FID?

FID and CLIPScore have been the main metrics for evaluating text-to-image synthesis. We performed an extra experiment where we explored a linear combination of these two metrics optimized on the COCO dataset. Although this combined metric achieved a non-trivial rank accuracy of 60%, its performance still lagged behind that of cFreD. More critically, when applied to the HPDv2 dataset, the combined metric’s rank accuracy lowered to 30%—worse than using FID or CLIPScore individually.

These results not only question the utility of combining FID and CLIPScore, but also highlight the inherent limitations of FID in capturing the text–image alignment necessary for the evaluation of text-to-image generation. Based on our experiments on PartiPrompts, HPDv2, and COCO, we argue that researchers should shift their focus towards monitoring cFreD and CLIPScore as the primary evaluation metrics.

4.4. Are we done with InceptionV3?

For this experiment, we include InceptionV3 as one of the backbones for cFreD. Our experimental results, summarized in Fig. 3, show a head-to-head comparison of each image backbone’s ranking of the diffusion models against the ground-truth ranking, reported as a “win rate”. Specifically, for each backbone, we measure how often its ranking of the diffusion models agrees with the actual human-derived ordering (win), disagrees (lose), or ties (split into both good

or both bad). Although InceptionV3 still secures a portion of wins, it lags behind newer transformer-based backbones, such as DINOv2-L/14 and ViT-L/16, which consistently achieve higher win rates and fewer mismatches. These findings suggest that, although InceptionV3 remains a good baseline, more advanced architectures yield rankings that better align with human judgment on the COCO dataset, reinforcing the move away from InceptionV3 in state-of-the-art text-to-image evaluations.

5. Ablations

To analyze how different image and text models affect cFreD, we experimented across all combinations of 43 different image models and 43 different text models to select the backbones for cFreD. The full list of these models is provided in the appendix. In this section, we specifically provide an in-depth analysis of how different visual encoder attributes impact cFreD’s correlation with human preferences. For each factor examined, we report the average correlation across all possible text encoders. We perform our ablations on the PartiPrompts Arena. Detailed results of these analyses are included in the appendix.

Effect of the size of the pre-training dataset on cFreD. Fig. 4a shows the correlation between cFreD and human preferences as a function of the size of the pre-training dataset for Vision Transformers (ViT). Larger datasets tend to improve alignment with human judgments, with models

trained on $\approx 10B$ images achieving the highest correlation of 0.79. Interestingly, the smallest dataset ($\approx 10M$) also demonstrates a strong correlation of 0.78, surpassing both the $\approx 2B$ (0.76) and $\approx 100M$ (0.73) categories. This non-monotonic relationship suggests that factors beyond raw data quantity, such as diversity and quality, significantly influence performance. Meanwhile, the $\approx 5B$ dataset yields the lowest correlation of 0.73. These findings emphasize the importance of both data scale and curation in optimizing text-conditioned image generation metrics.

Effect of image size on cFreD. Fig. 4b illustrates the correlation between cFreD and human preferences across varying input image resolutions. We observe a non-monotonic relationship: increasing resolutions do not consistently yield higher correlations. In particular, an image size of 299×229 (corresponding to the InceptionV3) achieves a high correlation of 0.760, while 518×518 (used in all DINOv2 models) reaches a correlation of 0.743. Smaller resolutions, such as 224×224 and 256×256 , still perform competitively at 0.719 and 0.701, respectively. However, beyond 518×518 , performance declines (e.g., 0.680 at 896×896 and 0.559 at 1024×1024).

Effect of ViT model size on cFreD. The correlation between cFreD and human preferences across Vision Transformer (ViT) sizes are presented in Fig. 4c. Larger models consistently achieve higher correlations, with the *Huge* category reaching the highest correlation of 0.786, followed closely by *Large* at 0.785. The smallest model (*Small*) achieves 0.755, indicating a performance gap compared to larger architectures. Intermediate model sizes (*Base*) yield correlations of 0.776, while *SO* (0.724) and *Giant* (0.755) show a gradual improvement between these model sizes.

Effect of ViT Feature dimensionality on cFreD. Fig. 4d shows the correlation between cFreD and human preferences across ViT feature dimensions from 256 to 1664. The relationship is non-monotonic: correlation peaks at 1024 features (0.79), while certain lower-dimensional representations (e.g., 640, 512, and 1280 features at 0.78) also perform strongly. Both very low (256 at 0.67) and very high (1536 at 0.75) feature sizes yield reduced correlations. These findings indicate that while increasing feature dimensionality generally improves alignment with human preferences, an optimal range exists where performance is maximized, suggesting a trade-off between model complexity and effective representation learning.

Effect of Zero-Shot ImageNet Accuracy on cFreD. Fig. 4e shows a boxplot of the correlation between cFreD and human preferences as a function of zero-shot ImageNet accuracy, evaluated exclusively on image-text pretrained models [18, 21, 55, 63, 75]. Higher zero-shot accuracies generally correspond to stronger correlations with human judgments, though variance exists within each accuracy level.

Models with the highest accuracy (81.37%) achieve the highest median correlation, while models at the lower end (51.53%) cluster around lower correlation values. These findings suggest that zero-shot ImageNet performance can serve as a useful indicator of downstream alignment with human preferences despite considerable variability among models with similar accuracy levels.

6. Discussion and Conclusion

In this work, we extend and repurpose Conditional Fréchet Inception Distance (cFID), first introduced in [66], for the evaluation of text-to-image generation. Recognizing key shortcomings in current evaluation practices—namely, reliance on outdated image encoders like InceptionV3 and the lack of explicit text-image alignment measures—we analyzed a range of modern vision and text backbone models. Our experiments show that modern transformer-based architectures (e.g., ViT, DINOv2, CLIP) significantly outperform InceptionV3, resulting in metrics that better align with human preferences. We replace the backbone models with a superior model and introduce cFreD.

Unlike traditional metrics such as FID or IS, which solely focus on image quality, cFreD explicitly measures semantic consistency between generated images and their corresponding text prompts, achieving higher correlation with human judgments. Additionally, our ablation studies reveal that optimal metric performance depends on balancing model complexity, data diversity, and representation quality, rather than simply scaling model size or dataset scale.

We advocate for cFreD as a robust, user-friendly metric for text-to-image synthesis evaluation. It delivers immediate, reliable assessments without constant updates or extensive human annotation. By open-sourcing our implementation and unified benchmarks, we aim to promote more systematic evaluations and accelerate generative model research.

There are several promising directions to extend the scope of cFreD. First, future research could explore combining cFreD with human preference-trained models by incorporating their image encoders as backbones within our metric. This hybrid approach leverages cFreD’s robust semantic alignment and human preference data’s fine-grained insights, offering the best of both. Second, while our current formulation is tailored for text-to-image synthesis, cFreD is inherently flexible and can be adapted to other conditional evaluation tasks. For example, it could be extended to assess image-to-text (captioning), text-to-video, or audio-to-video generation. Furthermore, cFreD can be generalized to condition on multiple inputs, such as in models like ControlNet [82] that require simultaneous conditioning on a text prompt and an image to generate a new image.

References

[1] Artificial Analysis. Text to image model arena. <https:////artificialanalysis.ai/text-to-image/arena?tab=Leaderboard>. Accessed: March 02, 2025. 2, 5

[2] Mahmoud Assran, Quentin Duval, Ishan Misra, Piotr Bojanowski, Pascal Vincent, Michael Rabbat, Yann LeCun, and Nicolas Ballas. Self-supervised learning from images with a joint-embedding predictive architecture. In *Proceedings of the IEEE/CVF Conference on Computer Vision and Pattern Recognition*, pages 15619–15629, 2023. 13

[3] Stella Biderman. Conditional fréchet inception distance. <https://x.com/BlancheMinerva/status/1757206462806343991>. Accessed: March 04, 2025. 1

[4] Tim Brooks, Aleksander Holynski, and Alexei A Efros. Instructpix2pix: Learning to follow image editing instructions. In *Proceedings of the IEEE/CVF conference on computer vision and pattern recognition*, pages 18392–18402, 2023. 1

[5] Tim Brooks, Bill Peebles, Connor Holmes, Will DePue, Yufei Guo, Li Jing, David Schnurr, Joe Taylor, Troy Luhman, Eric Luhman, Clarence Ng, Ricky Wang, and Aditya Ramesh. Video generation models as world simulators. 2024. 1

[6] Xinlei Chen, Hao Fang, Tsung-Yi Lin, Ramakrishna Vedantam, Saurabh Gupta, Piotr Dollár, and C Lawrence Zitnick. Microsoft coco captions: Data collection and evaluation server. *arXiv preprint arXiv:1504.00325*, 2015. 5

[7] Xinlei Chen, Saining Xie, and Kaiming He. An empirical study of training self-supervised vision transformers. In *Proceedings of the IEEE/CVF international conference on computer vision*, pages 9640–9649, 2021. 13

[8] Xiaokang Chen, Zhiyu Wu, Xingchao Liu, Zizheng Pan, Wen Liu, Zhenda Xie, Xingkai Yu, and Chong Ruan. Janus-pro: Unified multimodal understanding and generation with data and model scaling. *arXiv preprint arXiv:2501.17811*, 2025. 6

[9] Mehdi Cherti, Romain Beaumont, Ross Wightman, Mitchell Wortsman, Gabriel Ilharco, Cade Gordon, Christoph Schuhmann, Ludwig Schmidt, and Jenia Jitsev. Reproducible scaling laws for contrastive language-image learning. In *Proceedings of the IEEE/CVF conference on computer vision and pattern recognition*, pages 2818–2829, 2023. 13

[10] Wei-Lin Chiang, Lianmin Zheng, Ying Sheng, Anastasios Nikolas Angelopoulos, Tianle Li, Dacheng Li, Hao Zhang, Banghua Zhu, Michael Jordan, Joseph E. Gonzalez, and Ion Stoica. Chatbot arena: An open platform for evaluating llms by human preference, 2024. 2

[11] Hyung Won Chung, Le Hou, Shayne Longpre, Barret Zoph, Yi Tay, William Fedus, Yunxuan Li, Xuezhi Wang, Mostafa Dehghani, Siddhartha Brahma, et al. Scaling instruction-finetuned language models. *Journal of Machine Learning Research*, 25(70):1–53, 2024. 13

[12] Alexis Conneau, Kartikay Khandelwal, Naman Goyal, Vishrav Chaudhary, Guillaume Wenzek, Francisco Guzmán, Edouard Grave, Myle Ott, Luke Zettlemoyer, and Veselin Stoyanov. Unsupervised cross-lingual representation learning at scale. *arXiv preprint arXiv:1911.02116*, 2019. 13

[13] Jacob Devlin, Ming-Wei Chang, Kenton Lee, and Kristina Toutanova. Bert: Pre-training of deep bidirectional transform- ers for language understanding. In *Proceedings of the 2019 conference of the North American chapter of the association for computational linguistics: human language technologies, volume 1 (long and short papers)*, pages 4171–4186, 2019. 13

[14] Ming Ding, Wendi Zheng, Wenyi Hong, and Jie Tang. Cogview2: Faster and better text-to-image generation via hierarchical transformers. *Advances in Neural Information Processing Systems*, 35:16890–16902, 2022. 4

[15] Alexey Dosovitskiy, Lucas Beyer, Alexander Kolesnikov, Dirk Weissenborn, Xiaohua Zhai, Thomas Unterthiner, Mostafa Dehghani, Matthias Minderer, Georg Heigold, Sylvain Gelly, et al. An image is worth 16x16 words: Transformers for image recognition at scale. *arXiv preprint arXiv:2010.11929*, 2020. 13

[16] Patrick Esser, Robin Rombach, and Bjorn Ommer. Taming transformers for high-resolution image synthesis. In *Proceedings of the IEEE/CVF conference on computer vision and pattern recognition*, pages 12873–12883, 2021. 4

[17] Patrick Esser, Sumith Kulal, Andreas Blattmann, Rahim Entezari, Jonas Müller, Harry Saini, Yam Levi, Dominik Lorenz, Axel Sauer, Frederic Boesel, et al. Scaling rectified flow transformers for high-resolution image synthesis. In *Forty-first international conference on machine learning*, 2024. 1, 6

[18] Alex Fang, Albin Madappally Jose, Amit Jain, Ludwig Schmidt, Alexander Toshev, and Vaishaal Shankar. Data filtering networks. *arXiv preprint arXiv:2309.17425*, 2023. 8, 13

[19] Yuxin Fang, Wen Wang, Binhui Xie, Quan Sun, Ledell Wu, Xinggang Wang, Tiejun Huang, Xinlong Wang, and Yue Cao. Eva: Exploring the limits of masked visual representation learning at scale. In *Proceedings of the IEEE/CVF conference on computer vision and pattern recognition*, pages 19358–19369, 2023. 13

[20] Stephanie Fu, Netanel Tamir, Shobhita Sundaram, Lucy Chai, Richard Zhang, Tali Dekel, and Phillip Isola. Dreamsim: Learning new dimensions of human visual similarity using synthetic data. *arXiv preprint arXiv:2306.09344*, 2023. 2

[21] Samir Yitzhak Gadre, Gabriel Ilharco, Alex Fang, Jonathan Hayase, Georgios Smyrnis, Thao Nguyen, Ryan Marten, Mitchell Wortsman, Dhruba Ghosh, Jieyu Zhang, et al. Data-comp: In search of the next generation of multimodal datasets. *Advances in Neural Information Processing Systems*, 36: 27092–27112, 2023. 8, 13

[22] Ian Goodfellow, Jean Pouget-Abadie, Mehdi Mirza, Bing Xu, David Warde-Farley, Sherjil Ozair, Aaron Courville, and Yoshua Bengio. Generative adversarial nets. In *Advances in Neural Information Processing Systems*. Curran Associates, Inc., 2014. 1

[23] Shuyang Gu, Dong Chen, Jianmin Bao, Fang Wen, Bo Zhang, Dongdong Chen, Lu Yuan, and Baining Guo. Vector quantized diffusion model for text-to-image synthesis. In *Proceedings of the IEEE/CVF conference on computer vision and pattern recognition*, pages 10696–10706, 2022. 4

[24] Moayed Haji-Ali, Guha Balakrishnan, and Vicente Ordóñez. Elasticdiffusion: Training-free arbitrary size image generation through global-local content separation. In *Proceedings of*

the IEEE/CVF Conference on Computer Vision and Pattern Recognition, pages 6603–6612, 2024. 1

[25] Moayed Haji-Ali, Willi Menapace, Aliaksandr Siarohin, Guha Balakrishnan, Sergey Tulyakov, and Vicente Ordonez. Taming data and transformers for audio generation. *arXiv preprint arXiv:2406.19388*, 2024. 1

[26] Moayed Haji-Ali, Willi Menapace, Aliaksandr Siarohin, Ivan Skorokhodov, Alper Canberk, Kwot Sin Lee, Vicente Ordonez, and Sergey Tulyakov. Av-link: Temporally-aligned diffusion features for cross-modal audio-video generation. *arXiv preprint arXiv:2412.15191*, 2024. 1

[27] Kaiming He, Xinlei Chen, Saining Xie, Yanghao Li, Piotr Dollár, and Ross Girshick. Masked autoencoders are scalable vision learners. In *Proceedings of the IEEE/CVF conference on computer vision and pattern recognition*, pages 16000–16009, 2022. 13

[28] Sen He, Wentong Liao, Michael Ying Yang, Yongxin Yang, Yi-Zhe Song, Bodo Rosenhahn, and Tao Xiang. Context-aware layout to image generation with enhanced object appearance. In *Proceedings of the IEEE/CVF conference on computer vision and pattern recognition*, pages 15049–15058, 2021. 1

[29] Jack Hessel, Ari Holtzman, Maxwell Forbes, Ronan Le Bras, and Yejin Choi. Clipscore: A reference-free evaluation metric for image captioning. *arXiv preprint arXiv:2104.08718*, 2021. 1, 2, 5

[30] Martin Heusel, Hubert Ramsauer, Thomas Unterthiner, Bernhard Nessler, and Sepp Hochreiter. Gans trained by a two time-scale update rule converge to a local nash equilibrium. *Advances in neural information processing systems*, 30, 2017. 1, 2, 5

[31] Sadeep Jayasumana, Srikumar Ramalingam, Andreas Veit, Daniel Glasner, Ayan Chakrabarti, and Sanjiv Kumar. Rethinking fid: Towards a better evaluation metric for image generation. In *Proceedings of the IEEE/CVF Conference on Computer Vision and Pattern Recognition*, pages 9307–9315, 2024. 2, 5

[32] Diederik P. Kingma and Max Welling. Auto-encoding variational bayes. *International Conference on Learning Representations (ICLR)*, 2014. 1

[33] Alexander Kirillov, Eric Mintun, Nikhila Ravi, Hanzi Mao, Chloe Rolland, Laura Gustafson, Tete Xiao, Spencer Whitehead, Alexander C Berg, Wan-Yen Lo, et al. Segment anything. In *Proceedings of the IEEE/CVF international conference on computer vision*, pages 4015–4026, 2023. 13

[34] Yuval Kirstain, Adam Polyak, Uriel Singer, Shahbuland Matiania, Joe Penna, and Omer Levy. Pick-a-pic: An open dataset of user preferences for text-to-image generation. *Advances in Neural Information Processing Systems*, 36:36652–36663, 2023. 1, 2, 3

[35] Weijie Kong, Qi Tian, Zijian Zhang, Rox Min, Zuozhuo Dai, Jin Zhou, Jiangfeng Xiong, Xin Li, Bo Wu, Jianwei Zhang, et al. Hunyuanyvideo: A systematic framework for large video generative models. *arXiv preprint arXiv:2412.03603*, 2024. 1

[36] Max Ku, Dongfu Jiang, Cong Wei, Xiang Yue, and Wenhui Chen. Viescore: Towards explainable metrics for conditional image synthesis evaluation. *arXiv preprint arXiv:2312.14867*, 2023. 2

[37] Kuaishou. Kling video model. <https://kling.kuaishou.com/en>, 2024. 1

[38] Black Forest Labs. Flux. <https://github.com/black-forest-labs/flux>, 2024. 6

[39] Zhenzhong Lan, Mingda Chen, Sebastian Goodman, Kevin Gimpel, Piyush Sharma, and Radu Soricut. Albert: A lite bert for self-supervised learning of language representations. *arXiv preprint arXiv:1909.11942*, 2019. 13

[40] Donghoon Lee, Jiseob Kim, Jisu Choi, Jongmin Kim, Minwoo Byeon, Woonhyuk Baek, and Saehoon Kim. Karlo-v1.0.alpha on coyo-100m and cc15m. <https://github.com/kakaobrain/karlo>, 2022. 5

[41] Daiqing Li, Aleks Kamko, Ehsan Akhgari, Ali Sabet, Linmiao Xu, and Suhail Doshi. Playground v2.5: Three insights towards enhancing aesthetic quality in text-to-image generation, 2024. 6

[42] Tsung-Yi Lin, Michael Maire, Serge Belongie, James Hays, Pietro Perona, Deva Ramanan, Piotr Dollár, and C Lawrence Zitnick. Microsoft coco: Common objects in context. In *Computer vision–ECCV 2014: 13th European conference, zurich, Switzerland, September 6–12, 2014, proceedings, part v 13*, pages 740–755. Springer, 2014. 4

[43] Yaron Lipman, Ricky T. Q. Chen, Heli Ben-Hamu, Maximilian Nickel, and Matthew Le. Flow matching for generative modeling. In *The Eleventh International Conference on Learning Representations*, 2023. 1

[44] Xingchao Liu, Chengyue Gong, Lemeng Wu, Shujian Zhang, Hao Su, and Qiang Liu. Fusedream: Training-free text-to-image generation with improved clip+ gan space optimization. *arXiv preprint arXiv:2112.01573*, 2021. 4

[45] Yinhan Liu, Myle Ott, Naman Goyal, Jingfei Du, Mandar Joshi, Danqi Chen, Omer Levy, Mike Lewis, Luke Zettlemoyer, and Veselin Stoyanov. Roberta: A robustly optimized bert pretraining approach. *arXiv preprint arXiv:1907.11692*, 2019. 13

[46] Ge Ya Luo, Gian Mario Favero, Zhi Hao Luo, Alexia Jolicoeur-Martineau, and Christopher Pal. Beyond fvd: Enhanced evaluation metrics for video generation quality. *arXiv preprint arXiv:2410.05203*, 2024. 1

[47] Sicheng Mo, Fangzhou Mu, Kuan Heng Lin, Yanli Liu, Bochen Guan, Yin Li, and Bolei Zhou. Freecontrol: Training-free spatial control of any text-to-image diffusion model with any condition. In *Proceedings of the IEEE/CVF Conference on Computer Vision and Pattern Recognition*, pages 7465–7475, 2024. 1

[48] Alex Nichol, Prafulla Dhariwal, Aditya Ramesh, Pranav Shyam, Pamela Mishkin, Bob McGrew, Ilya Sutskever, and Mark Chen. Glide: Towards photorealistic image generation and editing with text-guided diffusion models. *arXiv preprint arXiv:2112.10741*, 2021. 2, 4

[49] OpenGenAI. Parti prompts leaderboard. <https://huggingface.co/spaces/OpenGenAI/parti-prompts-leaderboard>. Hugging Face Space. Accessed: March 02, 2025. 2, 5

[50] Maxime Oquab, Timothée Darcret, Théo Moutakanni, Huy Vo, Marc Szafraniec, Vasil Khalidov, Pierre Fernandez, Daniel Haziza, Francisco Massa, Alaaeldin El-Nouby, et al. Dinov2:

Learning robust visual features without supervision. *arXiv preprint arXiv:2304.07193*, 2023. 13

[51] Yuang Peng, Yuxin Cui, Haomiao Tang, Zekun Qi, Runpei Dong, Jing Bai, Chunrui Han, Zheng Ge, Xiangyu Zhang, and Shu-Tao Xia. Dreambench++: A human-aligned benchmark for personalized image generation. *arXiv preprint arXiv:2406.16855*, 2024. 2

[52] Pablo Pernias, Dominic Rampas, Mats Leon Richter, Christopher Pal, and Marc Aubreville. Würstchen: An efficient architecture for large-scale text-to-image diffusion models. In *The Twelfth International Conference on Learning Representations*, 2024. 5

[53] Dustin Podell, Zion English, Kyle Lacey, Andreas Blattmann, Tim Dockhorn, Jonas Müller, Joe Penna, and Robin Rombach. Sdxl: Improving latent diffusion models for high-resolution image synthesis. *arXiv preprint arXiv:2307.01952*, 2023. 1, 5, 6

[54] PromptHero. Prompthero. <https://prompthero.com/>. Accessed: March 04, 2025. 3

[55] Alec Radford, Jong Wook Kim, Chris Hallacy, Aditya Ramesh, Gabriel Goh, Sandhini Agarwal, Girish Sastry, Amanda Askell, Pamela Mishkin, Jack Clark, et al. Learning transferable visual models from natural language supervision. In *International conference on machine learning*, pages 8748–8763. PMLR, 2021. 8, 13, 14, 15

[56] Colin Raffel, Noam Shazeer, Adam Roberts, Katherine Lee, Sharan Narang, Michael Matena, Yanqi Zhou, Wei Li, and Peter J Liu. Exploring the limits of transfer learning with a unified text-to-text transformer. *Journal of machine learning research*, 21(140):1–67, 2020. 13

[57] Aditya Ramesh, Mikhail Pavlov, Gabriel Goh, Scott Gray, Chelsea Voss, Alec Radford, Mark Chen, and Ilya Sutskever. Zero-shot text-to-image generation. In *International conference on machine learning*, pages 8821–8831. Pmlr, 2021. 2

[58] Aditya Ramesh, Prafulla Dhariwal, Alex Nichol, Casey Chu, and Mark Chen. Hierarchical text-conditional image generation with clip latents. *arXiv preprint arXiv:2204.06125*, 1(2):3, 2022. 4

[59] Robin Rombach, Andreas Blattmann, Dominik Lorenz, Patrick Esser, and Björn Ommer. High-resolution image synthesis with latent diffusion models. In *Proceedings of the IEEE/CVF conference on computer vision and pattern recognition*, pages 10684–10695, 2022. 1, 4, 6

[60] RunwayML. Gen-3 alpha. <https://runwayml.com/research/introducing-gen-3-alpha>, 2024. 1

[61] Chitwan Saharia, William Chan, Saurabh Saxena, Lala Li, Jay Whang, Emily L Denton, Kamyar Ghasemipour, Raphael Gontijo Lopes, Burcu Karagol Ayan, Tim Salimans, et al. Photorealistic text-to-image diffusion models with deep language understanding. *Advances in neural information processing systems*, 35:36479–36494, 2022. 2

[62] Tim Salimans, Ian Goodfellow, Wojciech Zaremba, Vicki Cheung, Alec Radford, and Xi Chen. Improved techniques for training gans. *Advances in neural information processing systems*, 29, 2016. 1, 2

[63] Christoph Schuhmann, Romain Beaumont, Richard Vencu, Cade Gordon, Ross Wightman, Mehdi Cherti, Theo Coombes, Aarush Katta, Clayton Mullis, Mitchell Wortsman, et al. Laion-5b: An open large-scale dataset for training next generation image-text models. *Advances in neural information processing systems*, 35:25278–25294, 2022. 5, 8, 13

[64] Arseniy Shakhmatov, Anton Razzhigaev, Aleksandr Nikolic, Vladimir Arkhipkin, Igor Pavlov, Andrey Kuznetsov, and Denis Dimitrov. kandinsky 2.2, 2023. 5

[65] Jascha Sohl-Dickstein, Eric Weiss, Niru Maheswaranathan, and Surya Ganguli. Deep unsupervised learning using nonequilibrium thermodynamics. In *International conference on machine learning*, pages 2256–2265. pmlr, 2015. 1

[66] Michael Soloveitchik, Tzvi Diskin, Efrat Morin, and Ami Wiesel. Conditional frechet inception distance. *arXiv preprint arXiv:2103.11521*, 2021. 2, 4, 8

[67] George Stein, Jesse Cresswell, Rasa Hosseinzadeh, Yi Sui, Brendan Ross, Valentin Villecroze, Zhaoyan Liu, Anthony L Caterini, Eric Taylor, and Gabriel Loaiza-Ganem. Exposing flaws of generative model evaluation metrics and their unfair treatment of diffusion models. *Advances in Neural Information Processing Systems*, 36:3732–3784, 2023. 2, 5

[68] Andreas Steiner, Alexander Kolesnikov, Xiaohua Zhai, Ross Wightman, Jakob Uszkoreit, and Lucas Beyer. How to train your vit? data, augmentation, and regularization in vision transformers. *arXiv preprint arXiv:2106.10270*, 2021. 13

[69] Christian Szegedy, Vincent Vanhoucke, Sergey Ioffe, Jon Shlens, and Zbigniew Wojna. Rethinking the inception architecture for computer vision. In *Proceedings of the IEEE conference on computer vision and pattern recognition*, pages 2818–2826, 2016. 2, 13

[70] Lokesh Veeramacheneni, Moritz Wolter, Hildegard Kuehne, and Juergen Gall. Fr\`echet wavelet distance: A domain-agnostic metric for image generation. *arXiv preprint arXiv:2312.15289*, 2023. 2

[71] Zijie J Wang, Evan Montoya, David Munechika, Haoyang Yang, Benjamin Hoover, and Duen Horng Chau. Diffusiondb: A large-scale prompt gallery dataset for text-to-image generative models. *arXiv preprint arXiv:2210.14896*, 2022. 3

[72] Benjamin Warner, Antoine Chaffin, Benjamin Clavié, Orion Weller, Oskar Hallström, Said Taghadouini, Alexis Gallagher, Raja Biswas, Faisal Ladhak, Tom Aarsen, et al. Smarter, better, faster, longer: A modern bidirectional encoder for fast, memory efficient, and long context finetuning and inference. *arXiv preprint arXiv:2412.13663*, 2024. 13

[73] Xiaoshi Wu, Yiming Hao, Keqiang Sun, Yixiong Chen, Feng Zhu, Rui Zhao, and Hongsheng Li. Human preference score v2: A solid benchmark for evaluating human preferences of text-to-image synthesis. *arXiv preprint arXiv:2306.09341*, 2023. 2, 3, 5

[74] Xiaoshi Wu, Keqiang Sun, Feng Zhu, Rui Zhao, and Hongsheng Li. Human preference score: Better aligning text-to-image models with human preference. In *Proceedings of the IEEE/CVF International Conference on Computer Vision*, pages 2096–2105, 2023. 1, 2

[75] Hu Xu, Saining Xie, Xiaoqing Ellen Tan, Po-Yao Huang, Russell Howes, Vasu Sharma, Shang-Wen Li, Gargi Ghosh, Luke Zettlemoyer, and Christoph Feichtenhofer. Demystifying clip data. *arXiv preprint arXiv:2309.16671*, 2023. 8, 13

[76] Jiazheng Xu, Xiao Liu, Yuchen Wu, Yuxuan Tong, Qinkai Li, Ming Ding, Jie Tang, and Yuxiao Dong. Imagereward: Learning and evaluating human preferences for text-to-image generation. *Advances in Neural Information Processing Systems*, 36:15903–15935, 2023. [1](#), [2](#), [3](#), [5](#)

[77] Tao Xu, Pengchuan Zhang, Qiuyuan Huang, Han Zhang, Zhe Gan, Xiaolei Huang, and Xiaodong He. AttnGAN: Fine-grained text to image generation with attentional generative adversarial networks. In *Proceedings of the IEEE conference on computer vision and pattern recognition*, pages 1316–1324, 2018. [2](#)

[78] Zhuoyi Yang, Jiayan Teng, Wendi Zheng, Ming Ding, Shiyu Huang, Jiazheng Xu, Yuanming Yang, Wenyi Hong, Xiaohan Zhang, Guanyu Feng, et al. Cogvideox: Text-to-video diffusion models with an expert transformer. *arXiv preprint arXiv:2408.06072*, 2024. [1](#)

[79] Jiahui Yu, Yuanzhong Xu, Jing Yu Koh, Thang Luong, Gunjan Baid, Zirui Wang, Vijay Vasudevan, Alexander Ku, Yinfei Yang, Burcu Karagol Ayan, et al. Scaling autoregressive models for content-rich text-to-image generation. *arXiv preprint arXiv:2206.10789*, 2(3):5, 2022. [2](#)

[80] Xiaohua Zhai, Basil Mustafa, Alexander Kolesnikov, and Lucas Beyer. Sigmoid loss for language image pre-training. In *Proceedings of the IEEE/CVF international conference on computer vision*, pages 11975–11986, 2023. [13](#)

[81] Han Zhang, Tao Xu, Hongsheng Li, Shaoting Zhang, Xiaogang Wang, Xiaolei Huang, and Dimitris N Metaxas. Stackgan: Text to photo-realistic image synthesis with stacked generative adversarial networks. In *Proceedings of the IEEE international conference on computer vision*, pages 5907–5915, 2017. [2](#)

[82] Lvmin Zhang, Anyi Rao, and Maneesh Agrawala. Adding conditional control to text-to-image diffusion models. In *Proceedings of the IEEE/CVF international conference on computer vision*, pages 3836–3847, 2023. [1](#), [8](#)

[83] Richard Zhang, Phillip Isola, Alexei A Efros, Eli Shechtman, and Oliver Wang. The unreasonable effectiveness of deep features as a perceptual metric. In *Proceedings of the IEEE conference on computer vision and pattern recognition*, pages 586–595, 2018. [2](#)

[84] Sixian Zhang, Bohan Wang, Junqiang Wu, Yan Li, Tingting Gao, Di Zhang, and Zhongyuan Wang. Learning multi-dimensional human preference for text-to-image generation. In *Proceedings of the IEEE/CVF Conference on Computer Vision and Pattern Recognition*, pages 8018–8027, 2024. [2](#), [3](#), [5](#)

[85] Sixian Zhang, Bohan Wang, Junqiang Wu, Yan Li, Tingting Gao, Di Zhang, and Zhongyuan Wang. Learning multi-dimensional human preference for text-to-image generation. In *Proceedings of the IEEE/CVF Conference on Computer Vision and Pattern Recognition*, pages 8018–8027, 2024. [2](#)

[86] Yufan Zhou, Ruiyi Zhang, Changyou Chen, Chunyuan Li, Chris Tensmeyer, Tong Yu, Jiuxiang Gu, Jinhui Xu, and Tong Sun. Towards language-free training for text-to-image generation. In *Proceedings of the IEEE/CVF conference on computer vision and pattern recognition*, pages 17907–17917, 2022. [4](#)

A. Image and Text Backbone Models

In our experiments, we used 46 different image backbone models and 43 different text backbone models. For vision models, we employed those trained with self-supervised learning, including ViT trained on ImageNet-1k [15], ViT trained on ImageNet-21k [68], MAE [27], DINOv2 [50], MoCOv3 [7], and I-JEPA trained on both ImageNet-1k and ImageNet-22k [2]. We also incorporated image-and-text-aligned pretrained models such as CLIP [55], MetaCLIP [75], DFN-CLIP [18], OpenCLIP [9], DataComp-CLIP [21], ConvNeXT-CLIP [63], EVA02 [19], and SigLIP [80]. Additional image models included SAM-ViT [33] and Inception V3 [69]. For text models, we employed autoencoding models such as RoBERTa [45], BERT [13], ALBERT [39], ModernBERT [72], XLM-RoBERTa [12], as well as sequence-to-sequence models including FLAN-T5 [11] and T5 [56] were used. We also used the text encoders from the aforementioned image-and-text-aligned pretrained models. The complete lists of image and text backbone models used in our experiments are presented in Tables B.1 and B.2, respectively.

B. Analysis on Selecting Image and Text Backbone Models

We provide an in-depth analysis of how different image and text models affect cFreD. In our experiments, we tested all possible combinations of 43 different image and text models, focusing exclusively on ViT-based architectures and excluding SigLIP models with high-resolution options.

B.1. Spearman Correlation

We present Spearman correlation heatmaps that compare various text and image models across three distinct datasets: Parti-Prompts, HPDv2, and a random selection of COCO prompts.

Fig. B.1 showcases the heatmap on Parti-Prompts. Notably, certain image models such as ViT-B/16 trained on ImageNet-1K and ViT-H/14 trained on ImageNet-21K show consistently high performance with different text models. In contrast, SAM-ViT-H/16 presents more variability with different text models. While most ViT, DINO, and CLIP-based models demonstrate strong correlations across different text models, MAE models show slightly lower correlations.

Fig. B.2 presents the heatmap on HPDv2. Most models show strong correlations, whereas MAE models and SAM have lower correlations. Regardless of their performance levels, all image models show consistent correlation patterns across different text models.

Fig. B.3 provides the heatmap on randomly selected COCO prompts. The correlation values are significantly lower overall, ranging from approximately 0.00 to 0.30, which is much lower than both the Parti-Prompts and HPDv2

datasets. Most models show lower correlations, while only DINOv2 models consistently demonstrate stronger correlations. Compared to other datasets, this heatmap exhibits more variability, such as OpenCLIP showing a mixture of relatively higher and lower correlations depending on the text models.

These results highlight the importance of selecting compatible text and image models for improved cross-modal understanding, as not all combinations yield equally robust alignment. Additionally, it suggests that selecting a suitable image encoder plays a more pivotal role than choosing a text encoder, indicating that image encoder choice exerts a greater influence on overall performance.

B.2. Effect of Visual Encoders on HPDv2

In this section, we provide an analysis of how different visual encoder characteristics impact cFreD’s correlation with human preferences on HPDv2. For each factor examined, we report the average correlation across all possible text encoder combinations.

Effect of the size of the pre-training dataset on cFreD. Fig. B.4a shows the correlation between cFreD and human preferences as a function of the size of the pre-training dataset for Vision Transformer (ViT). In all ranges, it shows high alignment with human judgments, with a correlation higher than 0.95 correlation across all data sizes. This indicates that factors beyond raw data quantity, such as diversity and quality, significantly influence performance.

Effect of image size on cFreD. Fig. B.4b illustrates the correlation between cFreD and human preferences across varying input image resolutions. We observe a nonmonotonic relationship: increasing resolutions do not consistently yield higher correlations. In particular, an image size from 224x224 to 896x896 all achieves a high correlation above 0.96. However, beyond 518x518, performance declines, reaching 0.964 at 896x896 and showing the lowest correlation of 0.774 at 1024x1024.

Effect of ViT model size on cFreD. The correlation between cFreD and human preferences across Vision Transformer (ViT) sizes are presented in Fig. B.4c. It shows that all models achieve consistently high correlations—ranging from 0.945 to 0.986—indicating strong agreement with the target metric across scales. Interestingly, the *SO* model attains the highest correlation at 0.986, while *Gigantic* has the lowest, though still robust correlation of 0.945. The remaining models also cluster around correlations between 0.96 and 0.98, suggesting that simply increasing model size does not guarantee a strictly monotonic improvement in correlation.

Effect of ViT Feature dimensionality on cFreD. Fig. B.4d shows the correlation between cFreD and human preferences across ViT feature dimensions from 256 to 1664. The lowest number of the feature (256) shows the lowest correlation. However, we observe a clear plateau effect in performance

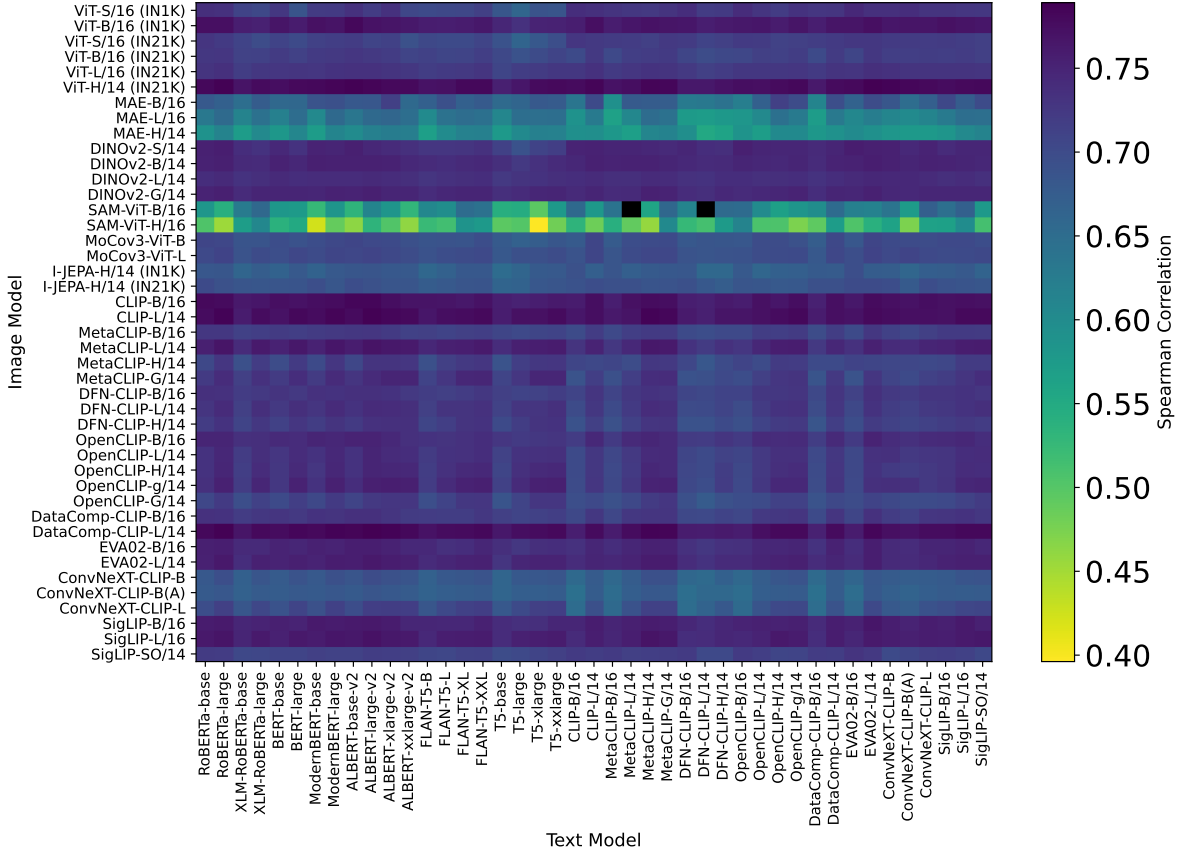


Figure B.1. Spearman Correlation Heatmap on Parti-Prompts.

once the feature count reaches 384, with correlation values stabilizing around 0.98-0.99 across a wide range of dimensionalities (512-1408). Interestingly, at extremely high dimensionalities (above 1536), we note a slight performance decline, with correlation dropping to 0.95 at 1664 features. This suggests an optimal range for feature dimensionality exists, beyond which additional computational complexity yields diminishing or even negative returns.

Effect of Zero-Shot ImageNet Accuracy on cFreD. Fig. B.4e depicts a boxplot of the correlation between cFreD and human preferences as a function of zero-shot ImageNet accuracy, evaluated exclusively on image-text pretrained models [55]. Higher zero-shot accuracies generally correspond to stronger correlations with human judgments, though variance exists within each accuracy bin. Interestingly, we find that correlations peak at a model with 66.58% zero-shot accuracy and decrease as model accuracy gets higher.

B.3. Effect of Visual Encoders on COCO prompts

In this section, we provide an analysis of how different visual encoder characteristics impact cFreD’s correlation with human preferences on randomly selected COCO prompts.

For each factor examined, we report the average correlation across all possible text encoder combinations.

Effect of the size of the pre-training dataset on cFreD. Fig. B.5a illustrates the correlation between cFreD and human preferences as a function of the pre-training dataset size for Vision Transformer (ViT). We observe a nonmonotonic relationship: increasing the pre-training dataset size does not consistently yield higher correlations. Notably, a model trained with fewer than 100 million samples achieves a high correlation of 0.33, while models trained with larger datasets show lower correlations ranging from 0.06 to 0.21. Interestingly, models trained with fewer than 5 billion samples demonstrate the lowest human correlation (0.06). These findings indicate that simply scaling up data does not guarantee improved performance for every metric or task, suggesting that balancing the quantity and quality of training data is crucial for optimal results.

Effect of image size on cFreD. Fig. B.4b illustrates the correlation between cFreD and human preferences across varying input image resolutions. We observe an inconsistent relationship: starting around 0.05 at an image size of 224x224, then rising to about 0.10 at 256x256 before dropping again to around 0.03 at 299x229. After a modest in-

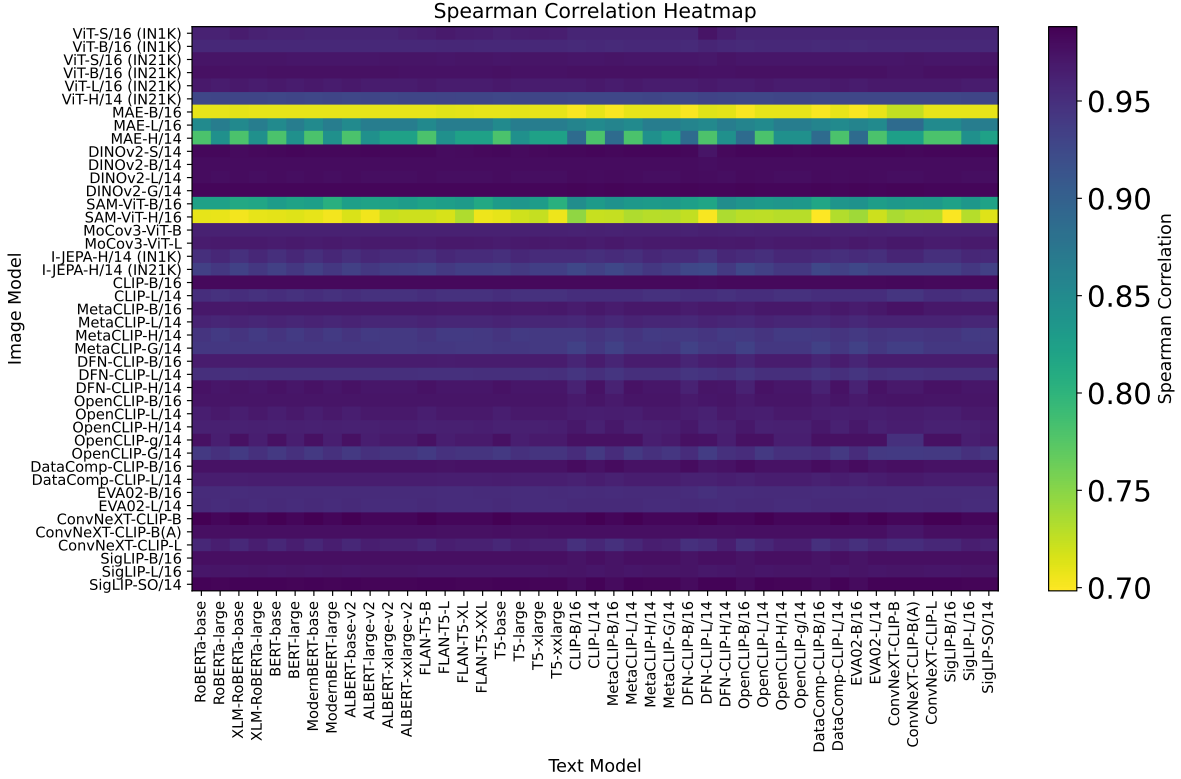


Figure B.2. Spearman Correlation Heatmap on HPDv2.

crease to 0.08 at 384x384, the correlation dips to 0.01 at 448x448 and then peaks sharply at 0.18 for an image size of 518x518. Beyond that, it decreases to nearly 0 at 896x896 and recovers slightly to 0.03 at 1024. These erratic trends suggest that there is no straightforward, monotonic relationship between image size and correlation for this particular task or metric, and the highest correlation appears in the midrange rather than at the smallest or largest resolutions.

Effect of ViT model size on cFreD. The correlation between cFreD and human preferences across Vision Transformer (ViT) sizes are presented in Fig. B.4c. Larger models tend to improve alignment with human judgments, with *Giant* model achieving the highest correlation of 0.320. However, when the model size gets bigger to *Gigantic* model, the correlation degrades down to 0.089. These results indicate that correlation does not simply increase in tandem with model size; rather, there seems to be an optimal range, as exemplified by the *Giant* model, for achieving the strongest alignment with the evaluation metric.

Effect of ViT Feature dimensionality on cFreD. Fig. B.4d shows the correlation between cFreD and human preferences across ViT feature dimensions from 256 to 1664. The two lowest numbers of the features (256 and 384) show the lowest correlation. However, we observe a clear plateau effect in performance once the feature count reaches 512,

with correlation values stabilizing around 0.30-0.32 across a wide range of dimensionalities (512-1152). Interestingly, at extremely high dimensionalities (above 1536), we note a slight performance decline, with correlation dropping to 0 at the 1408 feature. Although the correlation increases back to 0.32 with 1536 features, it decreases back to 0.14 at 1664 features. This suggests an optimal range for feature dimensionality exists, beyond which additional computational complexity yields diminishing or even negative returns.

Effect of Zero-Shot ImageNet Accuracy on cFreD. Fig. B.4e depicts a boxplot of the correlation between cFreD and human preferences as a function of zero-shot ImageNet accuracy, evaluated exclusively on image-text pretrained models [55]. Interestingly, we find that the lowest zero-shot accuracy has the highest correlation to human preference. However, after 68.58 of zero-shot accuracies, higher zero-shot accuracies generally correspond to stronger correlations with human judgments, though variance exists within each accuracy bin.

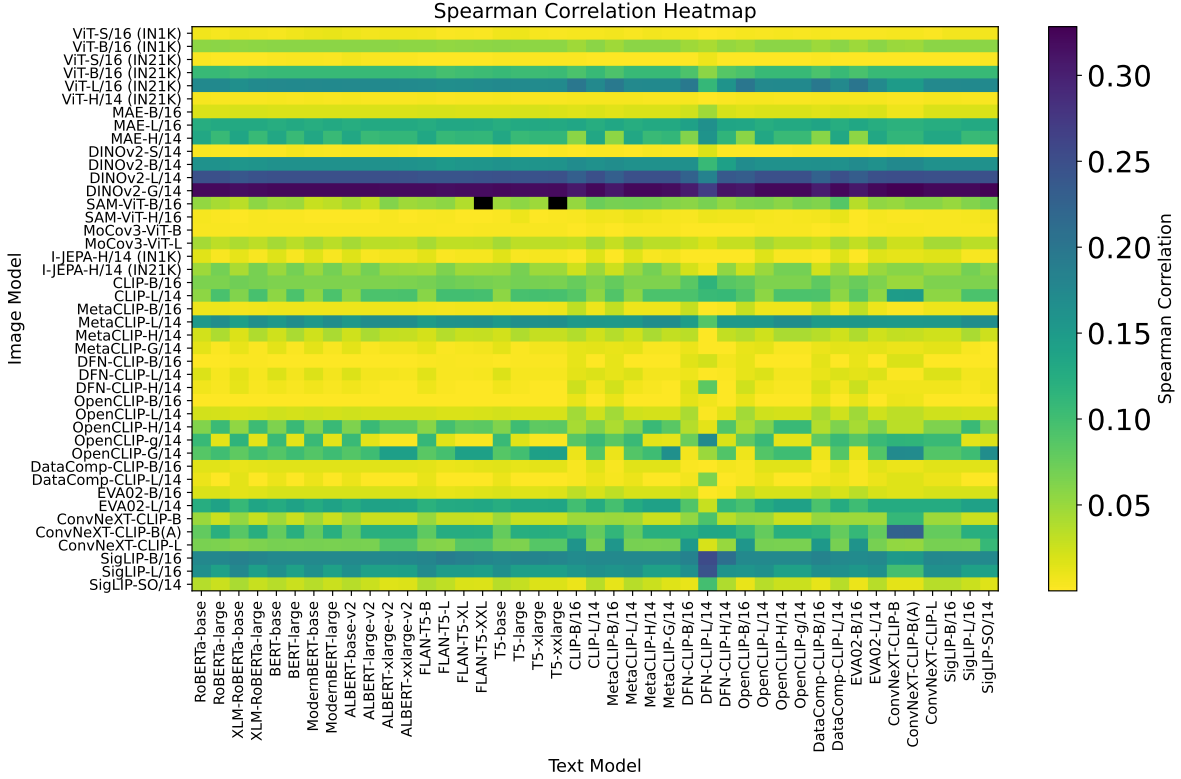


Figure B.3. Spearman Correlation Heatmap on random COCO prompts.

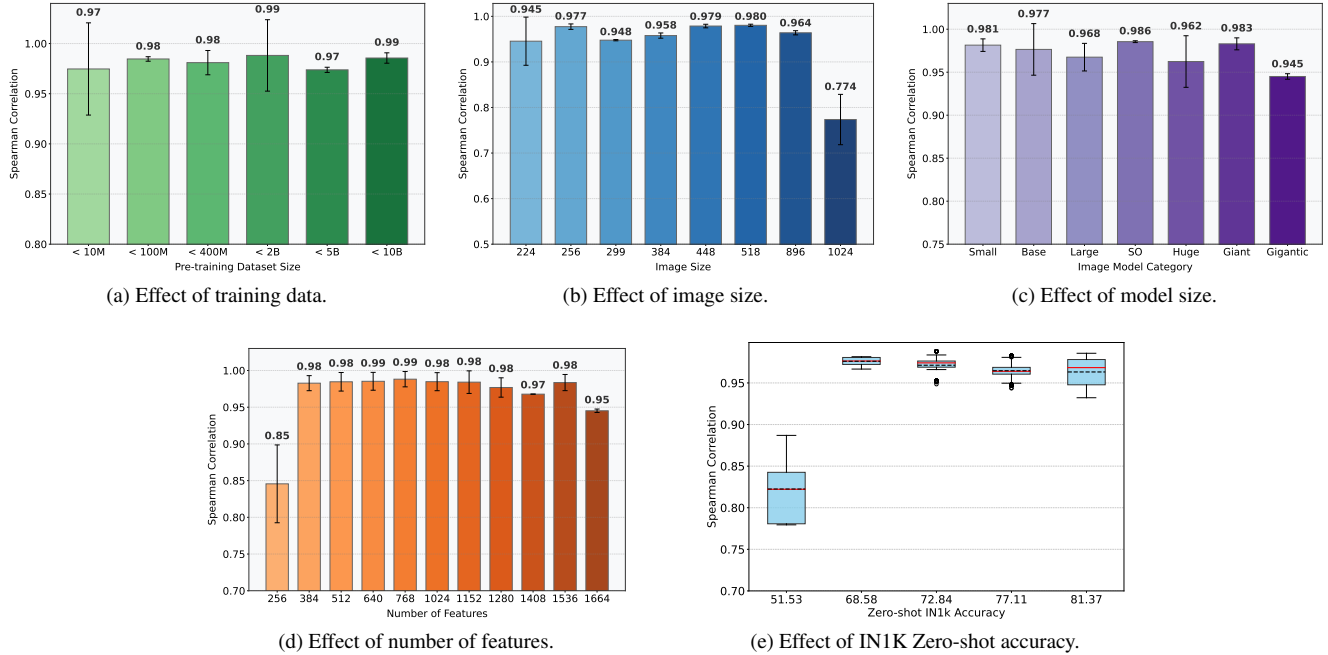


Figure B.4. **Ablation study on the HPDv2 dataset** comparing the correlation to human preferences under varying factors: (a) the ViT training dataset, (b) input image size, (c) model capacity, (d) the number of features in the last ViT layer, and (e) zero-shot accuracy on ImageNet-1K.

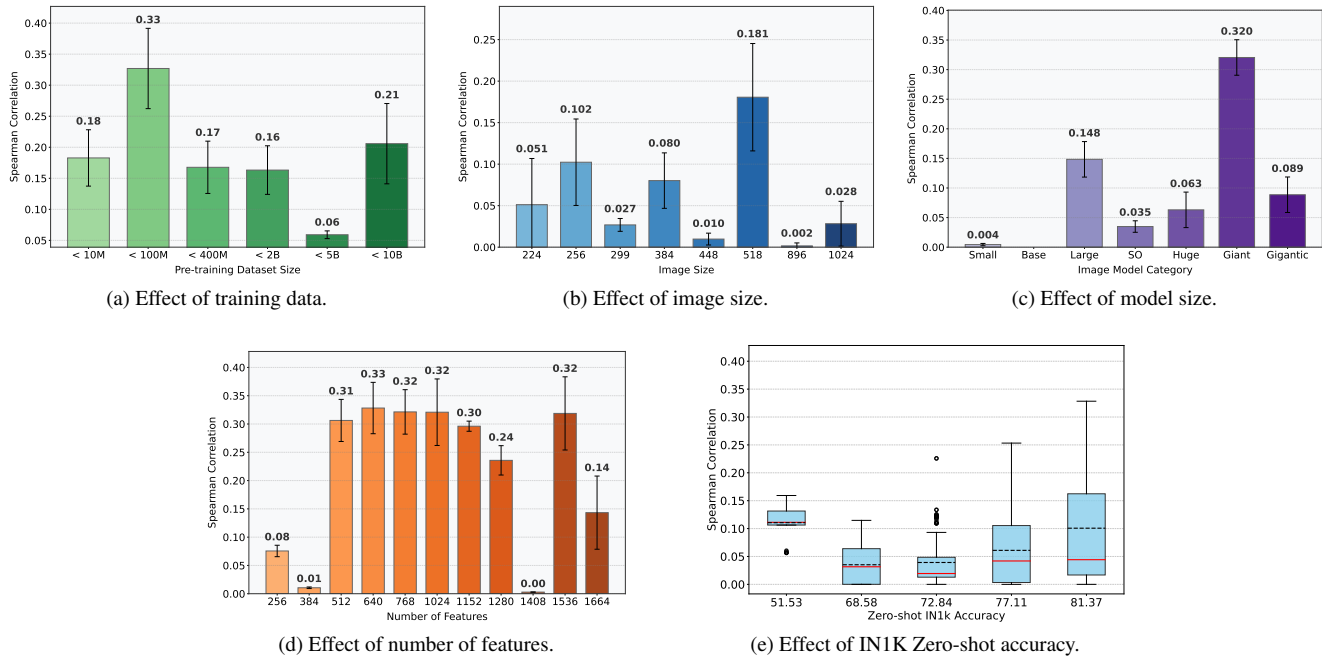


Figure B.5. Ablation study on randomly sampled COCO prompts comparing the correlation to human preferences under varying factors: (a) the ViT training dataset, (b) input image size, (c) model capacity, (d) the number of features in the last ViT layer, and (e) zero-shot accuracy on ImageNet-1K.

Model Name	Model Path
ViT-S/16 (IN1K)	timm/vit_small_patch16_224.augreg_in1k
ViT-B/16 (IN1K)	timm/vit_base_patch16_224.augreg_in1k
ViT-S/16 (IN21K)	timm/vit_small_patch16_224.augreg_in21k
ViT-B/16 (IN21K)	timm/vit_base_patch16_224.augreg_in21k
ViT-L/16 (IN21K)	timm/vit_large_patch16_224.augreg_in21k
ViT-H/14 (IN21K)	timm/vit_huge_patch14_224.orig_in21k
MAE-B/16	timm/vit_base_patch16_224.mae
MAE-L/16	timm/vit_large_patch16_224.mae
MAE-H/14	timm/vit_huge_patch14_224.mae
DINOv2-S/14	timm/vit_small_patch14_dinov2.lvd142m
DINOv2-B/14	timm/vit_base_patch14_reg4_dinov2.lvd142m
DINOv2-L/14	timm/vit_large_patch14_dinov2.lvd142m
DINOv2-G/14	timm/vit_giant_patch14_dinov2.lvd142m
SAM-ViT-B/16	timm/samvit_base_patch16
SAM-ViT-H/16	timm/samvit_huge_patch16
MoCov3-ViT-B	nyu-visionx/moco-v3-vit-b
MoCov3-ViT-L	nyu-visionx/moco-v3-vit-l
I-JEPA-H/14 (IN1K)	jmtzt/ijepa_vith14_1k
I-JEPA-H/14 (IN21K)	facebook/ijepa_vith14_22k
CLIP-B/16	timm/vit_base_patch16_clip_224.openai
CLIP-L/14	timm/vit_large_patch14_clip_224.openai
MetaCLIP-B/16	timm/vit_base_patch16_clip_224.metaclip_400m
MetaCLIP-L/14	timm/vit_large_patch14_clip_224.metaclip_400m
MetaCLIP-H/14	timm/vit_huge_patch14_clip_224.metaclip_altogether
MetaCLIP-G/14	timm/vit_gigantic_patch14_clip_224.metaclip_2pt5b
DFN-CLIP-B/16	timm/vit_base_patch16_clip_224.dfn2b
DFN-CLIP-L/14	timm/vit_large_patch14_clip_224.dfn2b
DFN-CLIP-H/14	timm/vit_huge_patch14_clip_224.dfn5b
OpenCLIP-B/16	timm/vit_base_patch16_clip_224.laion2b
OpenCLIP-L/14	timm/vit_large_patch14_clip_224.laion2b
OpenCLIP-H/14	timm/vit_huge_patch14_clip_224.laion2b
OpenCLIP-g/14	timm/vit_giant_patch14_clip_224.laion2b
OpenCLIP-G/14	timm/vit_gigantic_patch14_clip_224.laion2b
DataComp-CLIP-B/16	timm/vit_base_patch16_clip_224.datacompxl
DataComp-CLIP-L/14	timm/vit_large_patch14_clip_224.datacompxl
EVA02-B/16	timm/eva02_base_patch16_clip_224
EVA02-L/14	timm/eva02_large_patch14_clip_224
ConvNeXT-CLIP-B	timm/convnext_base.clip_laion2b
ConvNeXT-CLIP-B(A)	timm/convnext_base.clip_laiona
ConvNeXT-CLIP-L	timm/convnext_large_mlp.clip_laion2b_augreg
SigLIP-B/16	timm/vit_base_patch16_siglip_224.webli
SigLIP-L/16	timm/vit_large_patch16_siglip_256.webli
SigLIP-SO/14	timm/vit_so400m_patch14_siglip_gap_224.webli
InceptionV3	inception/inceptionv3
SigLIP-SO/14 (448)	timm/vit_so400m_patch14_siglip_gap_448.pali2_10b.pt
SigLIP-SO/14 (896)	timm/vit_so400m_patch14_siglip_gap_896.pali2_10b.pt

Table B.1. List of image backbone models used in our analysis.

Model Name	Model Path
RoBERTa-base	FacebookAI/roberta-base
RoBERTa-large	FacebookAI/roberta-large
XLM-RoBERTa-base	FacebookAI/xlm-roberta-base
XLM-RoBERTa-large	FacebookAI/xlm-roberta-large
BERT-base	google-bert/bert-base-uncased
BERT-large	google-bert/bert-large-uncased
ModernBERT-base	answerdotai/ModernBERT-base
ModernBERT-large	answerdotai/ModernBERT-large
ALBERT-base-v2	albert/albert-base-v2
ALBERT-large-v2	albert/albert-large-v2
ALBERT-xlarge-v2	albert/albert-xlarge-v2
ALBERT-xxlarge-v2	albert/albert-xxlarge-v2
FLAN-T5-B	google/flan-t5-base
FLAN-T5-L	google/flan-t5-large
FLAN-T5-XL	google/flan-t5-xl
FLAN-T5-XXL	google/flan-t5-xxl
T5-base	google/t5-v1_1-base
T5-large	google/t5-v1_1-large
T5-xlarge	google/t5-v1_1-xl
T5-xxlarge	google/t5-v1_1-xxl
CLIP-B/16	ViT-B-16-quickgelu.openai
CLIP-L/14	ViT-L-14-quickgelu.openai
MetaCLIP-B/16	ViT-B-16-quickgelu.metaclip_400m
MetaCLIP-L/14	ViT-L-14-quickgelu.metaclip_400m
MetaCLIP-H/14	ViT-H-14.metaclip_altogether
MetaCLIP-G/14	ViT-bigG-14-CLIPA.datacomp1b
DFN-CLIP-B/16	ViT-B-16-quickgelu.dfn2b
DFN-CLIP-L/14	ViT-L-14-quickgelu.dfn2b
DFN-CLIP-H/14	ViT-H-14-quickgelu.dfn5b
OpenCLIP-B/16	ViT-B-16.laion2b_s34b_b88k
OpenCLIP-L/14	ViT-L-14.laion2b_s32b_b82k
OpenCLIP-H/14	ViT-H-14.laion2b_s32b_b79k
OpenCLIP-g/14	ViT-g-14.laion2b_s34b_b88k
DataComp-CLIP-B/16	ViT-B-16.datacomp_xl_s13b_b90k
DataComp-CLIP-L/14	ViT-L-14.datacomp_xl_s13b_b90k
EVA02-B/16	EVA02-B-16.merged2b_s8b_b131k
EVA02-L/14	EVA02-L-14.merged2b_s4b_b131k
ConvNeXT-CLIP-B	convnext_base_w.laion2b_s13b_b82k_augreg
ConvNeXT-CLIP-B(A)	convnext_base_w.laion_aesthetic_s13b_b82k
ConvNeXT-CLIP-L	convnext_large_d.laion2b_s26b_b102k_augreg
SigLIP-B/16	ViT-B-16-SigLIP.webli
SigLIP-L/16	ViT-L-16-SigLIP-256.webli
SigLIP-SO/14	ViT-SO400M-14-SigLIP.webli

Table B.2. List of text backbone models used in our analysis.